

1 **Gap-Filling of Turbulent Heat Fluxes over Rice–Wheat-Rotation** 2 **Croplands Using the Random Forest Model**

3 Jianbin Zhang¹, Zexia Duan¹, Shaohui Zhou¹, Yubin Li¹, Zhiqiu Gao¹

4 ¹ School of Atmospheric Physics, Nanjing University of Information Science & Technology, Nanjing, 210044, China

5 *Correspondence to:* Dr. Yubin Li (liyubin@nuist.edu.cn)

6 **Abstract.** This study investigated the accuracy of the Random Forest (RF) model in gap-filling the sensible (H) and latent heat
7 (LE) fluxes, by using the observation data collected at a site over rice–wheat-rotation croplands in Shouxian County of eastern
8 China from 15 July 2015 to 24 April 2019. Firstly, the variable significances of the machine learning (ML) model’s five input
9 variables, including the net radiation (Rn), winds speed (WS), temperature (T), relative humidity (RH), and air pressure (P),
10 were examined, and it was found that Rn accounted for 78% and 76% of the total variable significance in H and LE calculating,
11 respectively, showing that it was the most important input variable. Secondly, the RF model’s accuracy with the five-variable
12 (Rn, WS, T, RH, P) input combination was evaluated, and the results showed that the RF model could reliably gap-fill the H
13 and LE with mean absolute errors (MAEs) of 5.88 Wm⁻² and 20.97 Wm⁻², and root mean square errors (RMSEs) of 10.67 Wm⁻²
14 and 29.46 Wm⁻², respectively. Thirdly, 4-variable input combinations were tested, and it was found that the best input
15 combination was (Rn, WS, T, P) by removing RH from the input list, and its MAE values of H and LE were reduced by 12.65%
16 and 7.12%, respectively. At last, through the Taylor diagram, H and LE gap-filling accuracies of the RF model, the support
17 vector machine (SVM) model, the k-nearest neighbor (KNN) model, and the gradient boosting decision tree (GBDT) model
18 were inter-compared, and the statistical metrics showed that RF was the most accurate for both H and LE gap-filling, while
19 the LR and KNN model performed the worst for H and LE gap-filling, respectively.

20

21 **1 Introduction**

22 The turbulent fluxes between the atmosphere and the ground play a crucial role in global climate change and atmospheric
23 circulation, and the inaccuracy of long-term observations of surface turbulent fluxes is a major factor in erroneous weather
24 predictions and climate projections. Research on the ecological effects of urban green spaces, agricultural ecosystems, and
25 forests all use surface turbulent fluxes as key indicators. Currently, the eddy covariance (EC) technique can be used to directly
26 measure the turbulent fluxes (Wilson et al., 2001; Jiang et al., 2021; Wang et al., 2021). However, due to sensor failure and
27 adverse meteorological factors (such as rainfall and frost), these high-frequency turbulence data are subject to errors (Khan et
28 al., 2018). As a result, it is difficult to obtain a continuous time series of ground-based turbulent fluxes. Furthermore, quality
29 assurance methods lead to unavailable sections of flux datasets (Nisa et al., 2021). Based on the above reasons, gap-filling is
30 in need to retrieve continuous datasets of EC-based fluxes. Researchers have developed approaches based on existing

31 meteorological information to fill up the gaps in atmospheric databases, such as interpolation, nonlinear regression, mean
32 diurnal method, and sampling techniques from the marginal distribution (Falge et al., 2001; Hui et al., 2004; Stauch et al.,
33 2006; Foltnov et al., 2020). Further, the ML technique has also become an effective method to be used in the calculation of
34 turbulent fluxes (McCandless et al., 2022).

35

36 As a result of recent developments in high computing technology, machine-learning-based algorithms have been developed
37 and successfully used in various areas, such as natural language processing, data mining, biometrics, computer vision, search
38 engines, clinical applications, video games, robots, etc. To address the missing data issue, machine-learning-based models
39 have recently been used to fill data gaps in meteorological elements and turbulent fluxes (Bianco et al., 2019; Yu et al., 2020).
40 As a result of their reliable and repeatable results, these models are now regarded as a standard gap-filling algorithm (Beringer
41 et al., 2017; Isaac et al., 2017). ML algorithms have several deficiencies even if they perform well in some areas. For instance,
42 over-fitting is a major concern that can occur when the training window is too short or the training dataset's quality is poor.
43 That's because the present ML approaches are not sufficiently adaptable to work in extreme situations with large values
44 (Kunwor et al., 2017; Moffat et al., 2007). Furthermore, even with the best technique, the model uncertainty of gap-filling still
45 plays a role, particularly when the gaps are relatively large. Numerous novel ML and optimization algorithms have been created
46 and put to use in numerous scientific domains since the 2000s, and their superiority has been demonstrated, either singly or as
47 a component of a hybrid or ensemble model (e.g. Gani et al., 2016).

48

49 Based on the need for fluxes dataset gap-filling, and the effectivity of the ML technique, this paper aims, firstly, to investigate
50 the performance of the RF machine learning algorithm trained from a dataset obtained over rice-wheat-rotation croplands in
51 Shouxian County, eastern China, in gap-filling the sensible and latent heat fluxes; and secondly, to analyze the RF model's
52 accuracy with various meteorological input combinations during training; and thirdly, to compare the performance of RF model
53 with other four typical ML models.

54

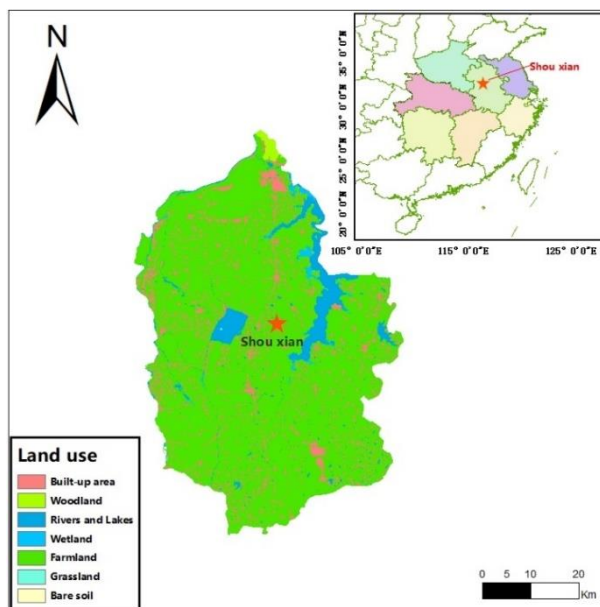
55 **2 Materials and Methods**

56 **2.1 Study area**

57 This observation was conducted at a site in Shouxian County in the eastern Chinese province of Anhui (32.42 °N, 116.76 °E)
58 (Figure 1). The altitude of the site is 27 meters, and the annual mean air temperature and annual cumulative precipitation here
59 are 16 °C and 1115 mm, respectively. Summer (from June to September) precipitation accounts for nearly 60% of the annual
60 precipitation amount, which meets the high water demand of rice. Drought sometimes occurs due to lack of precipitation in
61 the growing season of wheat. This observation site is rather flat, with farmland accounting for more than 90% of the area.
62 Winter wheat is grown here from November until late May, while from June to November the field is flooded, plowed, and

63 harrowed as rice paddies (Duan et al., 2021) (Figure 2). The subtropical northern boundary of the monsoon humid climatic
 64 type describes the area's climate.

65



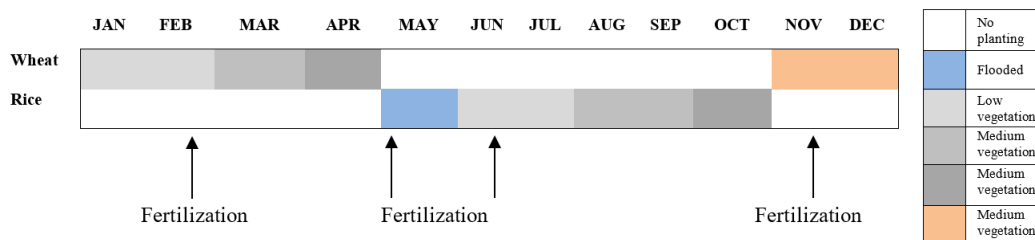
66

67

68

Figure 1. Geographical location and land-cover map of Shouxian County.

69



70

71

72

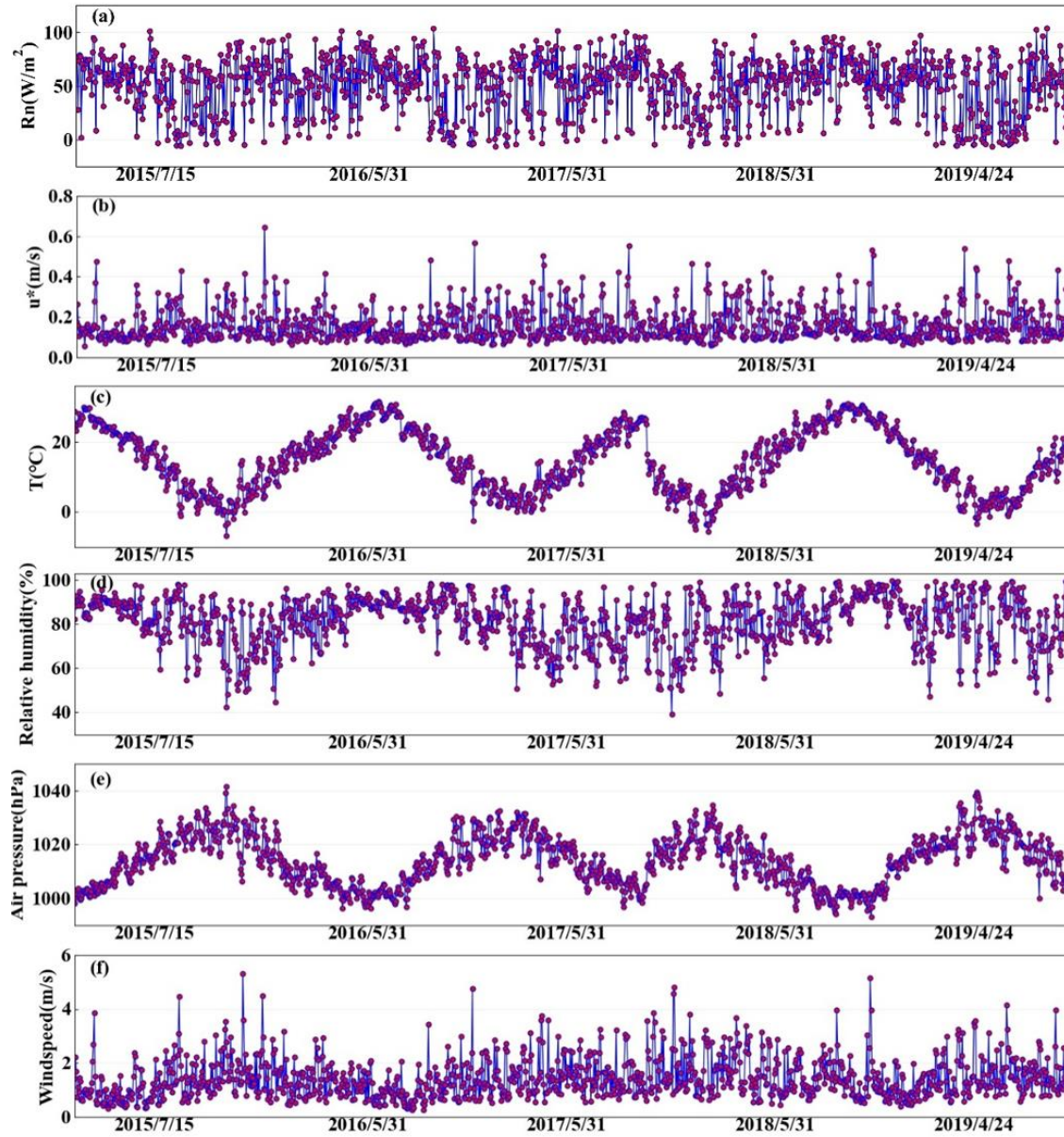
Figure 2. Crop calendars for the rice and wheat in the North Yangtze River Delta region.

73

74 2.2 Data

75 Over the site described above, EC sensors (EC 150, Campbell Scientific Inc., Logan, UT, USA) were installed at 2.5 meters
 76 above the ground, including a three-dimensional sonic anemometer (CSAT3, Campbell Scientific Inc., Logan, UT, USA) and
 77 a CO₂/H₂O open-path infrared gas analyzer. The sensible and latent heat fluxes were computed half-hourly using EddyPro

78 software, with time lag compensation, double coordinate rotation, spectrum correction, and Webb-Pearman-Leuning density
79 correction (Wutzler et al., 2018; Anapalli et al., 2019). Poor-quality fluxes (Eddypro quality check flag value=2) were
80 discarded. And a quality check based on the relationship between the measured flux and friction velocity was carried out to



81
82
83
84
85

Figure 3. Daily averaged a) Rn: net radiation(Wm^{-2}), b) u^* : friction velocity(m/s), c) T: air temperature($^{\circ}\text{C}$), d) RH: relative humidity(%), e) P: air pressure(hPa), and f) WS:wind speed(m s^{-1}).

86 remove the biased data (Papale et al., 2006). Then, using the marginal distribution sampling technique, the flow data were gap-
87 filled (Reichstein et al., 2005). The time series of air temperature, relative humidity, wind speed, air pressure, friction velocity,
88 and net radiation were also subjected to quality control. The missing data which need gapfilling are H and LE, with 7205 and
89 16013 missing, accounting for 12.09% and 26.87% respectively. According to the criteria of $X(h) < (X - 4\sigma)$ or $X(h) > (X +$
90 $4\sigma)$, where $X(h)$ indicates the time series of the component, X is the mean across the averaging interval, and σ is the standard
91 deviation, noisy data were eliminated (Gao et al., 2003). Data observed from 15 July 2015 to 24 April 2019 are used in this
92 study, and Figure 3 shows the daily average data of Rn: net radiation(W m^{-2}), u^* : friction velocity(m/s), T: air temperature($^{\circ}\text{C}$),
93 RH: relative humidity(%), P: air pressure(hPa), and WS: wind speed(m s^{-1}).
94

95 **2.3 The RF Model**

96 RF is a machine learning method that is quick, adaptable, and frequently used to analyze classification and regression jobs
97 (Breiman, 2001). This model can successfully evaluate highly dimensional and multicollinear data and is resistant to overfitting
98 (Belgiu et al., 2016). The RF model provides a feature-selection tool to assist in determining the importance of the predictor.
99 The contribution of each variable to the model, with important variables having a higher effect on the results of the model
100 evaluation, is the definition of feature significance (Liu et al., 2021). 90% of the data collected at the Shouxian observation
101 site throughout the study period were used to train the RF model, while the remaining 10% was used to independently validate
102 the model (hereafter, validation dataset). To lessen the overfitting in this case, a 10-fold cross-validation (CV) procedure was
103 used (Cai et al., 2020). All training data used here was randomly divided into ten subsamples of equal size for the 10-fold CV
104 tests. And nine out of the ten subsamples were used as training data (hereafter, training dataset), while the remaining subsample
105 was used as testing data (hereafter, testing dataset). All ten of the subsamples were utilized as testing data exactly once for
106 each of the 10 iterations of the CV procedure. One estimate was created by averaging the 10 findings from the folds. We
107 modified the four RF model hyperparameters based on Bayesian optimization to get the optimal model (Baareh et al., 2021;
108 Frazier, P.I., 2018): the maximum number of features considered to split a node (Max features), the maximum number of trees
109 to build (n estimators), the minimum sample number placed in a node prior to the node being split (min split), and the maximum
110 number of levels for each decision tree (Max depth). Bayesian optimizer is used to tune parameters, you can quickly find an
111 acceptable hyperparameter value, compared with grid search, the advantage is that the number of iterations is less (time saving),
112 the granularity can be very small. For example, if we want to adjust the regularized hyperparameters of linear regression, we
113 set the black box function to linear regression, the independent variable is a hyperparameter, the dependent variable is linear
114 regression in the training set accuracy, set an acceptable black box function dependent variable value, such as 0.95, the obtained
115 hyperparameter result is a hyperparameter that can make the linear regression accuracy exceed 0.95. The simulated
116 performance of the 10-fold CV outcomes was evaluated using four statistical metrics: the correlation coefficient (r), mean
117 absolute error (MAE), root mean square error (RMSE), and standard deviation(σ_n). As a result, the final RF model's parameters
118 were adjusted to n estimators = 246, min split = 2, Max features = 10, and Max depth = 35, to have the best statistical metrics.

119 The four statistical metrics are calculated by:

$$120 \quad r = \frac{\sum_{i=1}^N (S_i - \bar{S})(O_i - \bar{O})}{\sqrt{\sum_{i=1}^N (S_i - \bar{S})^2} \sqrt{\sum_{i=1}^N (O_i - \bar{O})^2}}, \quad (1)$$

121

$$122 \quad \text{MAE} = \frac{1}{N} \sum_{i=1}^N |S_i - O_i|, \quad (2)$$

123

$$124 \quad \text{RMSE} = \sqrt{\frac{\sum_{i=1}^N (S_i - O_i)^2}{N}}, \quad (3)$$

125

$$126 \quad \sigma_n = \sqrt{\frac{\sum_{i=1}^N (S_i - O_i)^2}{N}}. \quad (4)$$

127

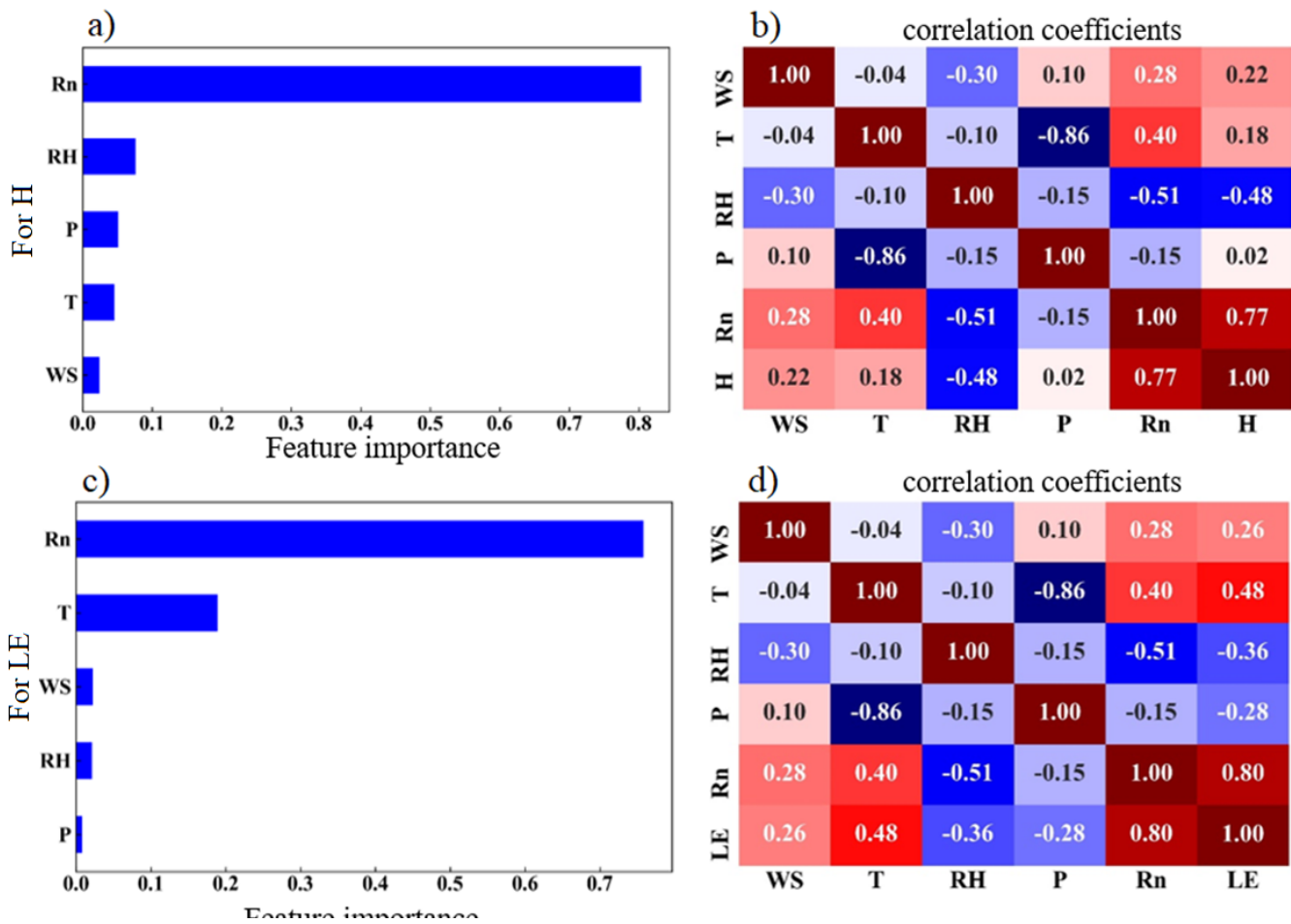
128 where S stands for the modeled value, O is the observation, \bar{O} is the mean observed value, and \bar{S} is the mean modeled
129 observation, σ_n indicates the standard deviation. The subscript i represents the serial number of samples, and N represents the
130 total number of samples.

131

132 **3 Results and discussion**

133 **3.1 Driving Factors of H and LE on a Seasonal Scale**

134 The possible driving factors of H and LE were investigated to determine their respective contributions by the RF model as
135 shown in Figure 4. Rn, which accounted for 78% and 76% of the total variable significance of H and LE, respectively, was the
136 most crucial variable in regulating the heat fluxes (Figures 4a and 4c). Consistent with the high variable significance values,
137 H and LE also had the highest r of 0.79 and 0.75 with H and LE, respectively, as shown in Figures 4b and 4d. The other four
138 factors contributed much smaller than Rn, and WS, T, RH, and P had importance values of 2%, 4%, 7%, and 5% (2.2%, 19%,
139 2%, and 0.6%) for H (LE), respectively. All these elements such as Rn, T, WS, RH are normalized before the model starts
140 training. When these elements are normalized, it ensures uniformity and comparability. In general, all of these predictors
141 played a role in the H and LE calculation, and for H, the sequence of importance was Rn, RH, P, T, and WS; while for LE, it
142 was Rn, T, WS, RH, and P. The most significant impact on the change of H and LE came from Rn, which was the most
143 important energy source of the surface and modulated the surface temperature directly. RH and T had a minor impact on the
144 H and LE changes in terms of climatic parameters, which carried the information of the light-dependent reactions of H and LE
145 fluxes. Particularly, WS and P had the minimal impacts on the H and LE fluxes. The WS, T, and RH also affected H and LE
146 according to the Monin-Obukhov similarity theory (Monin and Obukhov, 1954), while P represented the contributions from
147 the background weather systems.



148

149

150

151

Figure 4. The feature importance of the variables for a) H and c) LE, and the correlation coefficient between each of the input variables for b) H and d) LE.

152

3.2 RF Model Evaluation

153

154

155

156

157

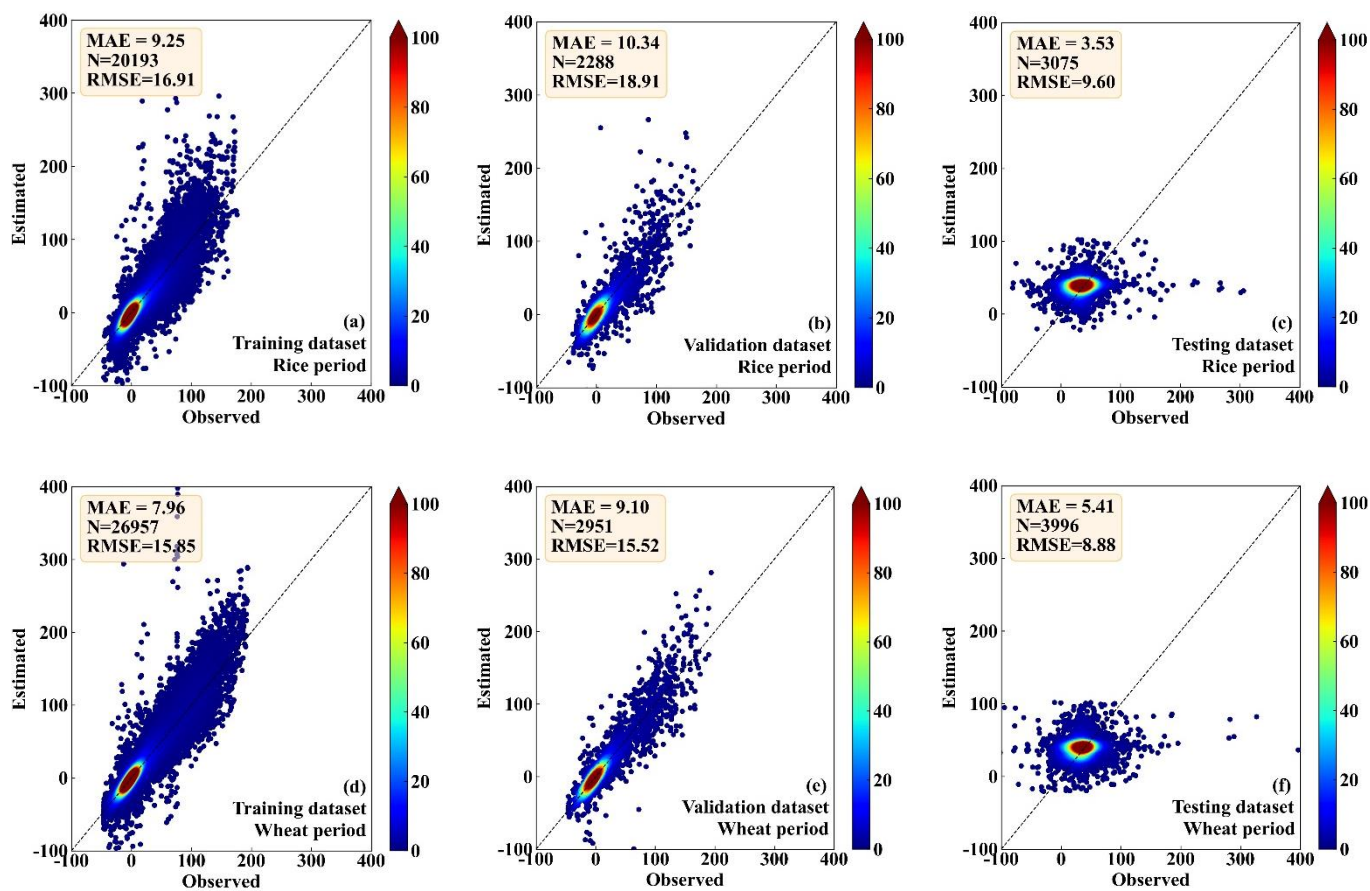
158

159

160

Figures 5-6 show the comparison between the observed and the RF-estimated H and LE, respectively. In the period of rice, the RF model showed good performance for both the training dataset (MAE=8.51 and 17.89 Wm⁻²; RMSE =14.11 and 29.82 Wm⁻², for H and LE, respectively) and the testing dataset (MAE =9.61 and 10.34 Wm⁻², RMSE = 15.63 and 17.21Wm⁻², for H and LE, respectively) (Figures 5a, 5b, 6a, and 6b). RF model also showed high consistency with direct measurements for the validation dataset (MAE=5.88 and 20.97 Wm⁻², RMSE = 10.67 and 29.46 Wm⁻², for H and LE, respectively), (Figures 5c and 6c). In the period of wheat, the performance of the RF model for the training, testing, and validation datasets of H and LE was similar to that in the period of rice. For the training, testing, and validation datasets, respectively, the MAEs are 7.18, 8.01, and 6.01 Wm⁻² for H, and 13.58, 8.82, and 19.93 Wm⁻² for LE; and the RMSEs are 12.27, 13.61, and 9.86 Wm⁻² for H, and

161 24.92, 15.17, and 28.74 Wm^{-2} for LE (Figure 5d,e,f, Figure 6 d,e,f). These results demonstrate that the RF model is capable of
162 effectively calculating the H and LE with input variables of Rn, WS, T, RH, and P.



163
164 **Figure 5.** Scatter density plots of the observed and the RF-estimated H values, a) and d) for the training dataset, b) and e) for the
165 validation dataset, and c) and f) for the testing dataset. And a), b) and c) are in the period of rice, while d), e) and f) are in the period
166 of wheat.

167

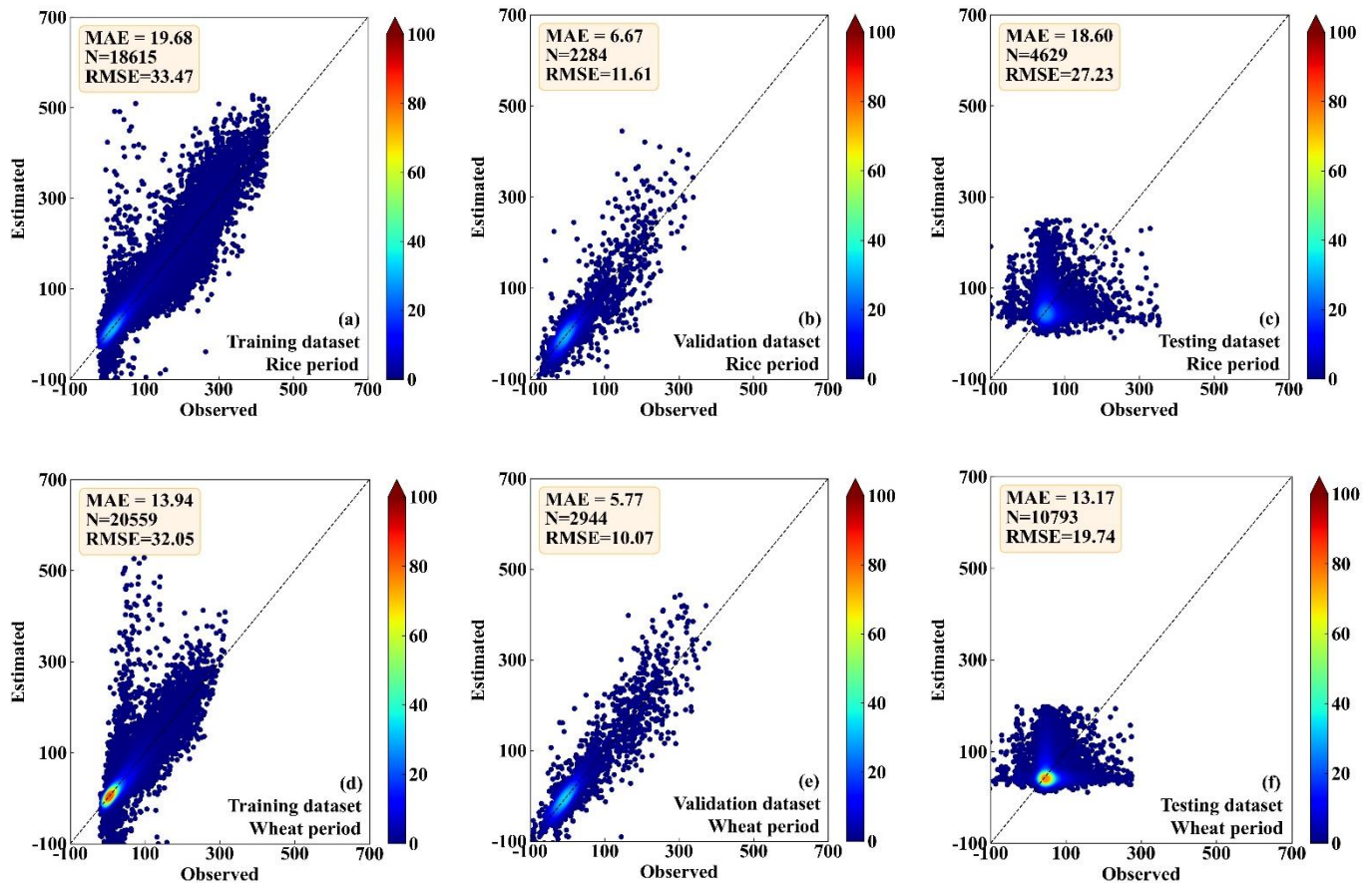


Figure 6. Same as Figure 5, but for LE.

168

169 3.3 Examination of Input Combinations

170 Meteorological elements may occasionally be unavailable due to the failure of sensors so the 5-variable input combination
 171 derived in Section 3.2 is not always applicable. Therefore, examination of other alternative input combinations is important to
 172 have substitute choices for data gap-filling when the 5-variable input combination is unavailable. In this subsection, we
 173 investigated the RF model's performance under the situation of lacking one element in the 5-variable input combination, i.e.,
 174 we tested the 4-variable input combinations of (WS, T, RH, P), (Rn, T, RH, P), (Rn, WS, RH, P), (Rn, WS, T, P), and (Rn,
 175 WS, T, RH), by removing Rn, WS, T, RH, and P from the 5-variable input combination, respectively. The MAEs and RMSEs
 176 for these combinations are shown in Table 1, and it demonstrates that the RF model's accuracy may either increase or decrease
 177 as a result of the removal of a meteorological element during the training phase. For instance, it was found that the model's
 178 performance greatly improved once RH was eliminated from the input combination, with the MAE and RMSE of H decreasing
 179 from 6.48 and 11.94 Wm^{-2} to 5.66 and 11.06 Wm^{-2} , respectively, and LE from 19.1 and 39.39 Wm^{-2} to 17.74 and 35.27 Wm^{-2} .
 180 ². This outcome is logical given that RH and H do not have a strong correlation, as a result, performance will be enhanced if

181 RH is not included in the gap-filling processing pipeline. According to our findings, the RF model's performance may be
182 greatly enhanced by excluding irrelevant meteorological elements from the study and choosing only those that have a
183 significant impact on the variable. Our findings imply that in order to attain the best gap-filling accuracy, it is necessary to
184 take into account both the advantages and disadvantages of ML-based models as well as the ideal input components. The results
185 suggested that RH at a single level was not well correlated to the fluxes as shown in Section 3.1, because the one-level RH
186 was strongly affected by the irrigation activity which was an external factor of the weather system. As a result, RF model
187 performance was enhanced when the irrelevant variable (i.e., RH) was removed from the input list. The same condition also
188 happened to the removal of WS, as could be seen from Section 3.1, WS showed small correlations with the fluxes. WS over
189 this site was rather small, and frequently below 2 m s^{-1} , and under this light wind condition, the fluxes were mostly driven by
190 the buoyancy rather than the wind shear. Figure 7 presents the MAE variation percentage of the 4-variable input combinations
191 from the 5-variable input combination. After RH was removed from the input list, the RF model showed favorable performance
192 for both H and LE, as shown in Figure 7, with MAE values improvements of 12.65 and 7.12%, respectively. Notably, the
193 removal of Rn from the input combination resulted in a considerable decline in the RF model's performances, with MAE
194 degradation percentage values reaching 16.20% and 10.73%, respectively. This outcome makes sense since Rn is highly
195 associated with H and LE; hence, performance will be declined if Rn is left out of the input training dataset. As a consequence,
196 our findings demonstrated that choosing strongly associated components could greatly increase the gap-filling accuracy.
197 According to our findings, the best input combination is (Rn, WS, T, P).

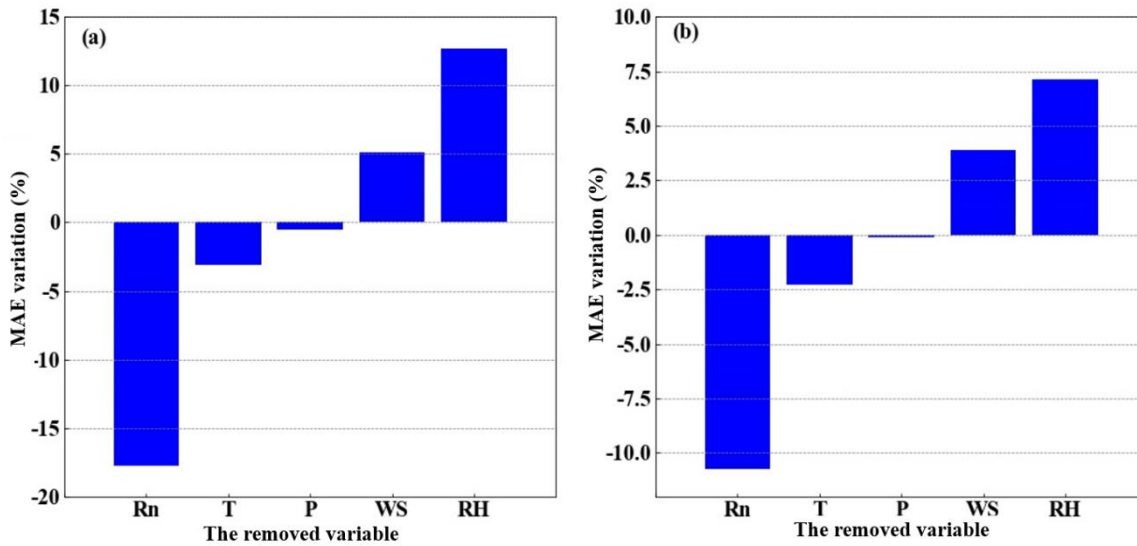
198

199 **Table 1. The MAEs and RMSEs of the RF-estimated heat fluxes for the 4-variable input combinations, and the corresponding**
200 **changes from the 5-variable input combination.**

201

Factors Included	Factors Eliminated		MAE (change)	RMSE (change)
WS, T, RH, P	Rn	H	7.63 (+1.15)	10.72 (-1.22)
		LE	21.15 (+2.05)	39.38 (-4.62)
Rn, T, RH, P	WS	H	6.15 (-0.33)	11.42 (-0.52)
		LE	18.36 (-0.74)	36.13 (-2.34)
Rn, WS, RH, P	T	H	6.68 (+0.20)	11.48 (-0.46)
		LE	19.54 (+0.44)	38.54 (-1.46)
Rn, WS, T, P	RH	H	5.66 (-0.82)	11.06 (-0.88)
		LE	17.74 (-1.36)	35.27 (-4.12)
Rn, WS, T, RH	P	H	6.49 (+0.03)	11.77 (-0.17)
		LE	19.12 (+0.02)	38.13 (-1.07)

202



203

204

205 **Figure 7. The MAE percentage variation after changing the 5-variable input combinations to the 4-variable input combinations, a)**
 206 **for H, and b) for LE, respectively. The x-axis labels indicate the removed variables.**

207

208 It should be noted that other variables that might have an impact on the H and LE were not investigated here. For example,
 209 given that our research site was over farmland and plants were growing, knowledge of the variations of the leaf area index
 210 (LAI) and inclusion of it to the training dataset should also be useful to increase the accuracy of the RF model in H and LE
 211 gap-filling. The monsoonal climate here also incurred considerable precipitation variations, which might as well potentially
 212 contribute to the RF model accuracy improvement. However, due to the lack of LAI and precipitation observations, the
 213 inclusion of the two variables into the RF model training dataset was not applicable in this study. Additionally, as shown above,
 214 more variables would bring a higher observation demand, and lead to more complexity and potentially decreased results, such
 215 as the adding variable of RH.

216

217 3.4 Comparison with other four ML methods

218 3.4.1 Comparison in H estimation

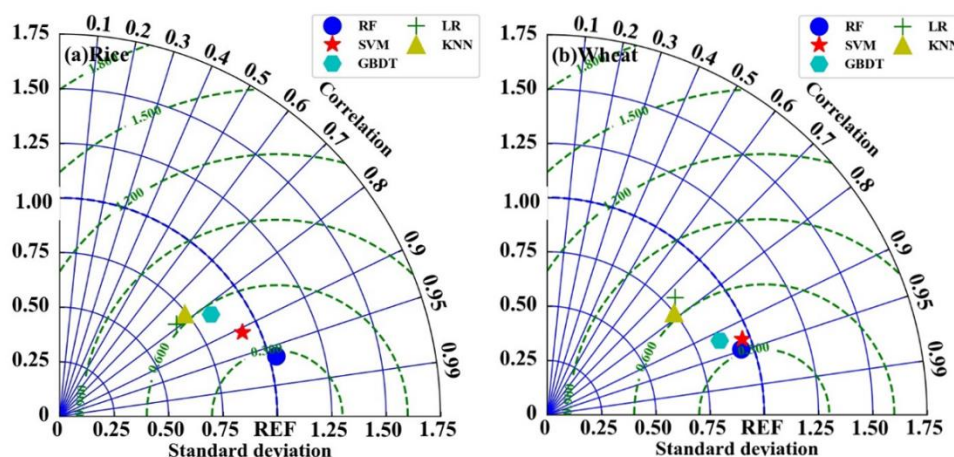
219

220 To further investigate the reliability of the RF model, we used a Taylor diagram to compare its performance in H estimation
 221 with other four ML models: support vector machine (SVM), k-nearest neighbor (KNN), gradient boosting decision tree
 222 (GBDT), and linear regression (LR). SVM is a data-oriented classification algorithm, and the basic model is to find the best
 223 separation hyperplane on the feature space so that the positive and negative sample intervals on the training set are maximum.
 224 Its advantages are that the kernel function can be used to map to a high-dimensional space; the use of the kernel function can

225 solve the nonlinear classification ; the classification idea is very simple, that is, to maximize the interval between the sample
 226 and the decision-making surface ;the classification effect is better ;and the nonlinear relationship between data and features is
 227 easy to obtain when the small and medium-sized sample size is large.KNN is particularly suitable for multi-classification
 228 problems. Its advantage is that it is simple in thought, easy to understand, easy to implement; No estimation parameters, no
 229 training; High accuracy, insensitive to outliers.GBDT can flexibly handle various types of data, including continuous and
 230 discrete values. With relatively few parameter adjustment times, the prediction preparation rate can also be relatively high. If
 231 the data dimension is high, the computational complexity of the algorithm will increase. Using some robust loss functions, the
 232 robustness to outliers is very strong.LR is a statistical analysis method that uses regression analysis in mathematical statistics
 233 to determine the quantitative relationship between two or more variables that depend on each other.The results have good
 234 interpretability, can intuitively express the importance of each attribute in the prediction, and the calculation of entropy is not
 235 complicated.

236 All the models were optimized with the same technique described above for the RF model. The results are shown in Figure 8.
 237 The EC measurements were used as the benchmark. It can be seen that the RF model generally outperforms the other four
 238 models, with the standard deviations (σ_n) and correlation values of 1.05 and 0.98 during the period of rice planting, and 0.96
 239 and 0.95 during the period of wheat planting, respectively. The SVM model is the second most accurate model, with the σ_n and
 240 correlation of 0.92 and 0.98 during the period of rice planting, and 0.91 and 0.93 during the period of wheat planting,
 241 respectively. The LR model performs the worst, with the σ_n and correlation of 0.60 and 0.76 during the period of rice planting,
 242 and 0.80 and 0.72 during the period of wheat planting, respectively. The accuracy of KNN and the GBDT models is in between
 243 the above-discussed models, and the σ_n and correlation during the rice and wheat period for KNN are 0.68 and 0.73, and 0.77
 244 and 0.82; and for GBDT are 0.79 and 0.80, and 0.81 and 0.9, respectively.

245



246

247

248

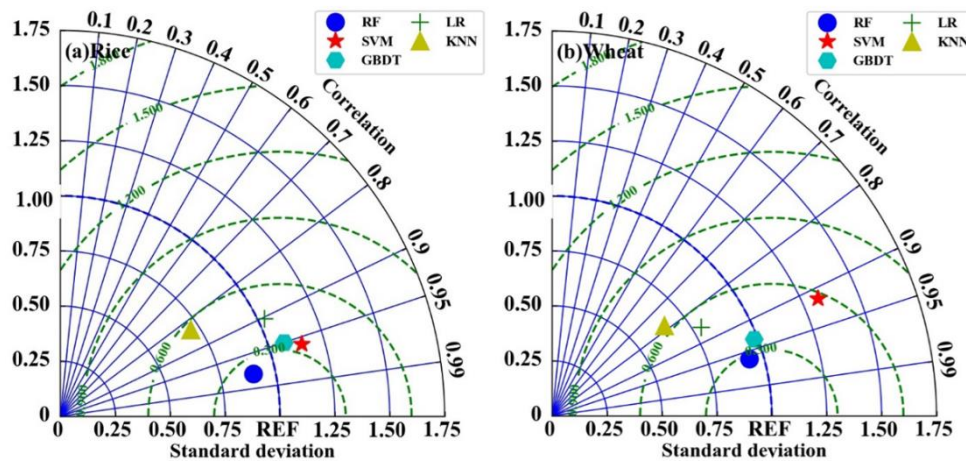
Figure 8. The performances of the five models for estimating H in the period of a) rice and b) wheat.

249

250 3.4.2 Comparison in LE estimation

251

252 Figure 9 illustrates a comparison of the estimated LE by all five models during the period of rice and wheat planting. The
253 results are similar to those in the H estimation, and the RF model is found to perform better than the other four models, with
254 the σ_n and correlation values of 0.95 and 0.97 during the period of rice planting, and 0.97 and 0.96 during the period of wheat
255 planting, respectively. Nonetheless, the KNN model performs the worse for LE estimating and has the σ_n and correlation
256 values of 0.68 and 0.82 during the period of rice planting, and 0.62 and 0.79 during the period of wheat planting, respectively.
257 Overall, as shown by the Taylor diagram of Figures 8 and 9, in this study the RF model has the best accuracy in either H or
258 LE estimation for data gap-filling.



259

260

261

262

Figure 9. Same as Figure 8, but for LE

263 4 Summary and Conclusions

264 To assess the RF model's capacity for gap-filling the sensible and latent heat flux measurements over rice-wheat rotation
265 croplands, 90% of the total observation data gathered at Shouxian were utilized for training and testing, and the remaining 10%
266 for independent validation. Our findings demonstrate that R_n is the most important variable in regulating H and LE, and it
267 accounts for 78% and 76% of the total variable significance in the RF model construction for H and LE calculation, respectively.
268 The least important variables are WS and P, and their total variable significances are 2% and 0.6%, respectively. During the
269 periods of rice and wheat planting, the RF model with a 5-variable input combination shows reliable performance, with MAE
270 values of 5.88 Wm^{-2} and 20.97 Wm^{-2} , and RMSE values of 10.67 Wm^{-2} and 29.46 Wm^{-2} , respectively. However, further
271 analysis of the RF model with 4-variable input combinations indicates that the performance of the model is improved when

272 RH is removed from the input list, and the MAE values decrease by 12.65% and 7.12% for H and LE, respectively. Nonetheless,
273 the 4- variable input combination without Rn causes an increase in the MAE values of the model, by 16.20% and 10.73% for
274 H and LE, respectively. Therefore, the best input combination found in this study for heat fluxes gap-filling is (Rn, WS, T, P).
275 Statistical comparison of RF and other four typical ML models (LR, KNN, SVN, and GBDT) by Tylar diagram further shows
276 that RF is the most accurate, with the standard deviations and correlation values of 0.95 and 0.97 during the period of rice
277 planting, and 0.97 and 0.96 during the period of wheat planting, respectively. While the LR and KNN models perform the
278 worst for H and LE gap-filling, respectively, according to the statistical metrics of the Tylor diagram.

279

280 This study is based on only the data collected over rice–wheat-rotation croplands, but the method presented above to find a
281 reliable gap-filling ML model can also be used over other types of the underlying surface and in other climate zones. It should
282 be noted that over different types of the underlying surface and climates, the variable significances can vary and a careful
283 check of the input combinations is needed. For example, over polar oceans with strong winds, Rn probably is not the most
284 important driving factor, while the winds which cause mostly the turbulence may take the first place. On the other hand, over
285 areas without human irrigation activity, RH will possibly be strongly related to the latent heat flux, and hence the inclusion of
286 it into the input list may increase the ML model performance. Besides the examination of the input combinations, the choice
287 of an ML model and the method to optimize its parameters are also important.

288

289 Overall, this study shows the potential to use the RF model to produce trustworthy gap-filling data of H and LE over rice–
290 wheat-rotation croplands, and the ML methods are suggested to be used to derive the fluxes' estimations when direct EC
291 observations are not available.

292

293 **References**

294 Alavi, N., Warland, J.S., Berg, A.A.: Filling gaps in evapotranspiration measurements for water budget studies: Evaluation of
295 a Kalman filtering approach, *J. Agric. For. Meteorol.*, 141 (1), 57–66, <https://doi.org/10.1016/j.agrformet.2006.09.011>,
296 2006.

297 Anapalli, S.S.; Fisher, D.K.; Reddy, K.N.; Krutz, J.L.; Pinnamaneni, S.R.; Sui, R.: Quantifying water and CO₂ fluxes and water
298 use efficiencies across irrigated C3 and C4 crops in a humid climate, *J. Sci. Total Environ.*, 663, 338–350,
299 <https://doi.org/10.1016/j.scitotenv.2018.12.471>, 2018.

300 Baareh, A.K.; Elsayad, A.; Al-Dhaifallah, M.: Recognition of splice-junction genetic sequences using random forest and
301 Bayesian optimization, *J. Multimed. Tools Appl.*, 80, 30505–30522, <https://doi.org/10.1007/s11042-021-10944-7>, 2021.

302 Belgiu, M.; Dragut, L.: Random forest in remote sensing: A review of applications and future directions, *Isprs J. Photogramm.*
303 *J.Remote Sensing.*, 114, 24–31, <https://doi.org/10.1016/j.isprsjprs.2016.01.011>, 2016.

304 Beringer, J., McHugh, I., Hutley, L. B., Isaac, P., and Kljun, N.: Technical note: Dynamic INtegrated Gap-filling and
305 partitioning for OzFlux (DINGO), *J. Biogeosciences.*, 14, 1457–1460, <https://doi.org/10.5194/bg-14-1457-2017>, 2017.

306 Best, M. J., M. Pryor, D. B. Clark, G. G. Rooney, et al.: The Joint UK Land Environment Simulator (JULES), model description
307 - Part 1: Energy and water fluxes, *J. Geosci. Model Dev.*, 4, 677–699, <https://doi.org/10.5194/gmd-4-677-2011>, 2011.

308 Bianco, M.J.; Gerstoft, P.; Traer, J.; Ozanich, E.; Roch, M.A.; Gannot, S.; Deledalle, C.-A.: Machine learning in acoustics:
309 Theory and applications, *J. Acoust. Soc. Am.*, 146, 3590–3628, <https://doi.org/10.1121/1.5133944>, 2019.

310 Breiman, L.: Random Forests, *J. Mach. Learn.*, 45, 5–32, <https://doi.org/10.1023/A:1010933404324>, 2001.

311 Cai, J.C.; Xu, K.; Zhu, Y.H.; Hu, F.; Li, L.H.: Prediction and analysis of net ecosystem carbon exchange based on gradient
312 boosting regression and random forest, *J. Appl. Energy.*, 262, 114566, <https://doi.org/10.1016/j.apenergy.2020.114566>,
313 2020.

314 Duan, Z.; Grimmond, C.; Gao, C.Y.; Sun, T.; Liu, C.; Wang, L.; Li, Y.; Gao, Z.: Seasonal and interannual variations in the
315 surface energy fluxes of a rice–wheat rotation in Eastern China, *J. Appl. Meteorol. Climatol.*, 60, 877–891,
316 <https://doi.org/10.1175/JAMC-D-20-0233.1>, 2021.

317 Duan, Z.; Yang, Y.; Wang, L.; Liu, C.; Fan, S.; Chen, C.; Tong, Y.; Lin, X.; Gao, Z.: Temporal characteristics of carbon
318 dioxide and ozone over a rural-cropland area in the Yangtze River Delta of eastern China, *J. Sci. Total Environ.*, 757,
319 e143750, <https://doi.org/10.1016/j.scitotenv.2020.143750>, 2021.

320 Falge, E.; Baldocchi, D.; Olson, R.; Anthoni, P.; Aubinet, M.; Bernhofer, C.; Burba, G.; Ceulemans, R.; Clement, R.; Dolman,
321 H.: Gap filling strategies for defensible annual sums of net ecosystem exchange, *J. Agric. For. Meteorol.*, 107, 43–69,
322 [https://doi.org/10.1016/S0168-1923\(00\)00225-2](https://doi.org/10.1016/S0168-1923(00)00225-2), 2001.

323 Foltýnová L.; Fischer, M.; McGloin, R.P.: Recommendations for gap-filling eddy covariance latent heat flux measurements
324 using marginal distribution sampling, *J. Theor. Appl. Climatol.*, 139, 677–688, <https://doi.org/10.1007/s00704-019-02975-w>, 2020.

326 Frazier, P.I.: A Tutorial on Bayesian Optimization, arXiv 2018, <https://doi.org/10.48550/arXiv.1807.02811>, 2018.

327 Gao, Z. Q., L. G. Bian, and X. J. Zhou.: Measurements of turbulent transfer in the near-surface layer over a rice paddy in China,
328 *J. Geophys. Res.*, 108(D13), 4387–4387, <https://doi.org/10.1029/2002JD002779>, 2003.

329 Garratt, J. R.: The atmospheric boundary layer. Cambridge Atmospheric and Space Science Series, Cambridge University
330 Press, 316, <https://doi.org/10.1017/CBO9781316117422>, 2015.

331 Hui, D.; Wan, S.; Su, B.; Katul, G.; Monson, R.; Luo, Y.: Gap-filling missing data in eddy covariance measurements using
332 multiple imputation (MI) for annual estimations, *J. Agric. For. Meteorol.*, 121, 93–111, [https://doi.org/10.1016/S0168-1923\(03\)00158-8](https://doi.org/10.1016/S0168-1923(03)00158-8), 2004.

334 Isaac, P., Cleverly, J., McHugh, I., Van Gorsel, E., Ewenz, C., and Beringer, J.: OzFlux data: Network integration from
335 collection to curation, *J. Biogeosciences*, 14, 2903–2928, <https://doi.org/10.5194/bg-14-2903-2017>, 2017.

336 Jiang, L.; Zhang, B.; Han, S.; Chen, H.; Wei, Z.: Upscaling evapotranspiration from the instantaneous to the daily time scale:
337 Assessing six methods including an optimized coefficient based on worldwide eddy covariance flux network, *J. Hydrol.*,
338 596, 126135, <https://doi.org/10.1016/j.jhydrol.2021.126135>, 2021.

339 Kepert, J.: Choosing a boundary layer parameterization for tropical cyclone modelling, *J. Mon. Wea. Rev.* [serial online].,
340 140(5), 1427-1445, DOI: <https://doi.org/10.1175/MWR-D-11-00217.1>, 2012.

341 Khan, M.S.; Jeon, S.B.; Jeong, M.H.: Gap-Filling Eddy Covariance Latent Heat Flux: Inter-Comparison of Four Machine
342 Learning Model Predictions and Uncertainties in Forest Ecosystem, *J. Remote Sens.*, 13, 4976.
343 <https://doi.org/10.3390/rs13244976>, 2021.

344 Khan, M.S.; Liaqat, U.W.; Baik, J.; Choi, M.: Stand-alone uncertainty characterization of GLEAM, GLDAS and MOD16
345 evapotranspiration products using an extended triple collocation approach, *J. Agric. For. Meteorol.*, 252, 256–268,
346 <https://doi.org/10.1016/j.agrformet.2018.01.022>, 2018.

347 Kim, Y.; Johnson, M.S.; Knox, S.H.; Black, T.A.; Dalmagro, H.J.; Kang, M.; Kim, J.; Baldocchi, D.: Gap-filling approaches
348 for eddy covariance methane fluxes: A comparison of three machine learning algorithms and a traditional method with
349 principal component analysis, *J. Glob. Chang. Biol.*, 26, 1499–1518, <https://doi.org/10.1111/gcb.14845>, 2020.

350 Kunwor, S., Starr, G., Loescher, H. W., and Staudhammer, C. L.: Preserving the variance in imputed eddy covariance
351 measurements: Alternative methods for defensible gap filling, *J. Agr. Forest Meteorol.*, 232, 635–649,
352 <https://doi.org/10.1016/j.agrformet.2016.10.018>, 2017.

353 Li, X., Z. Gao, Y. Li, and B. Tong.: Comparison of sensible heat fluxes measured by a large aperture scintillometer and eddy
354 covariance system over a heterogeneous farmland in East China, *J. Atmosphere.*, 8, 101, <https://doi.org/10.3390/atmos8060101>, 2017.

356 Liu, J.; Zuo, Y.; Wang, N.; Yuan, F.; Zhu, X.; Zhang, L.; Zhang, J.; Sun, Y.; Guo, Z.; Guo, Y.; et al.: Comparative Analysis
357 of Two Machine Learning Algorithms in Predicting Site-Level Net Ecosystem Exchange in Major Biomes, *J. Remote
358 Sens.*, 13, 2242, <https://doi.org/10.3390/rs13122242>, 2021.

359 McCandless, T., Gagne, D. J., Kosović, B., Haupt, S. E., Yang, B., Becker, C., & Schreck, J. (2022). Machine Learning for
360 Improving Surface-Layer-Flux Estimates. *Boundary-Layer Meteorology*, 185(2), 199-228.

361 Moffat, A. M., Papale, D., Reichstein, M., Hollinger, D. Y., Richardson, A. D., Barr, A. G., Beckstein, C., Braswell, B. H.,
362 Churkin G., Desai, A. R., Falge, E., Gove, J. H., Heimann, M., Hui, D., Jarvis, A. J., Kattge, J., Noormets, A., and Stauch,
363 V. J.: Comprehensive comparison of gap-filling techniques for eddy covariance net carbon fluxes, *J. Agr. Forest Meteorol.*,
364 147, 209–232, <https://doi.org/10.1016/j.agrformet.2007.08.011>, 2007.

365 Moncrieff, J.; Clement, R.; Finnigan, J.; Meyers, T.: Averaging, Detrending, and Filtering of Eddy Covariance Time Series.
366 In *Handbook of Micrometeorology: A Guide for Surface Flux Measurement and Analysis*, The Netherlands, pp., 7–31,
367 https://doi.org/10.1007/1-4020-2265-4_2, 2006.

368 Monin, A. S., & Obukhov, A. M. (1954). Basic laws of turbulent mixing in the surface layer of the atmosphere. *Contrib.*
369 *Geophys. Inst. Acad. Sci. USSR*, 151(163), e187.

370 Nisa, Z.; Khan, M.S.; Govind, A.; Marchetti, M.; Lasserre, B.; Magliulo, E.; Manco, A.: Evaluation of SEBS, METRIC-
371 EEFlux, and QWaterModel Actual Evapotranspiration for a Mediterranean Cropping System in Southern Italy, *J. Remote*
372 *Sens.*, 13, 4976–18 of 19, <https://doi.org/10.3390/agronomy11020345>, 2021.

373 Papale, D.; Reichstein, M.; Aubinet, M.; Canfora, E.; Bernhofer, C.; Kutsch, W.; Longdoz, B.; Rambal, S.; Valentini, R.;
374 Vesala, T.; et al.: Towards a standardized processing of Net Ecosystem Exchange measured with eddy covariance
375 technique: Algorithms and uncertainty estimation, *J. Biogeosciences.*, 3, 571–583, <https://doi.org/10.5194/bg-3-571-2006>,
376 2006.

377 Reichstein, M.; Falge, E.; Baldocchi, D.; Papale, D.; Aubinet, M.; Berbigier, P.; Bernhofer, C.; Buchmann, N.; Gilmanov, T.;
378 Granier, A.; et al.: On the separation of net ecosystem exchange into assimilation and ecosystem respiration: Review and
379 improved algorithm, *J. Glob. Change Biol.*, 11, 1424–1439, <https://doi.org/10.1111/j.1365-2486.2005.001002.x>, 2005.

380 Richard, A.; Fine, L.; Rozenstein, O.; Tanny, J.; Geist, M.; Pradalier, C.: Filling Gaps in Micro-Meteorological Data,
381 Switzerland, https://doi.org/10.1007/978-3-030-67670-4_7, 2020.

382 Stauch, V.J.; Jarvis, A.J.: A semi-parametric gap-filling model for eddy covariance CO₂ flux time series data, *J. Glob. Chang.*
383 *Biol.*, 12, 1707–1716, <https://doi.org/10.1111/j.1365-2486.2006.01227.x>, 2006.

384 Vitale, D.; Bilancia, M.; Papale, D.: A multiple imputation strategy for eddy covariance data, *J. Environ. Inform.*, 34, 68–87,
385 <https://doi.org/10.3808/jei.201800391>, 2018.

386 Wang, L.; Wu, B.; Elnashar, A.; Zeng, H.; Zhu, W.; Yan, N.: Synthesizing a Regional Territorial Evapotranspiration Dataset
387 for Northern China, *J. Remote Sens.*, 13, 1076, <https://doi.org/10.3390/rs13061076>, 2021.

388 Webb, E.K.; Pearman, G.I.; Leuning, R. Correction of flux measurements for density effects due to heat and water vapor
389 Transfer, *Q. J. R. Meteorol. Soc.*, 106, 85–100, <https://doi.org/10.1002/qj.49710644707>, 1980.

390 Wilson, K.B.; Hanson, P.J.; Mulholland, P.J.; Baldocchi, D.D.; Wullschlegel, S.D.: A comparison of methods for determining
391 forest evapotranspiration and its components: Sap-flow, soil water budget, eddy covariance and catchment water balance,
392 *J. Agric. For. Meteorol.*, 106, 153–168, [https://doi.org/10.1016/S0168-1923\(00\)00199-4](https://doi.org/10.1016/S0168-1923(00)00199-4), 2001.

393 Wutzler, T.; Lucas-Moffat, A.; Migliavacca, M.; Knauer, J.; Sickel, K.; Sigut, L.; Reichstein, M.: Basic and extensible post-
394 processing of eddy covariance flux data with REddyProc, *J. Biogeosciences.*, 15 (16): 5015–5030,
395 <https://doi.org/10.5194/bg-15-5015-2018>, 2018.

396 Yu, T.C.; Fang, S.Y.; Chiu, H.S.; Hu, K.S.; Tai, P.H.Y.; Shen, C.C.F.; Sheng, H.: Pin accessibility prediction and optimization
397 with deep learning-based pin pattern recognition, *J. IEEE Trans. Comput.-Aided Des. Integr. Circuits Syst.*, 40, 2345–
398 2356, <https://doi.org/10.1145/3316781.3317882>, 2019.